# Correlation of superconductivity with crystal structure in (NH_{3})_{y}Cs_{x}FeSe

Lu Zheng, Xiao Miao, Yusuke Sakai, Hidenori Goto, Eri Uesugi, Ritsuko Eguchi, Saki Nishiyama, Kunihisa Sugimoto, Akihiko Fujiwara, and Yoshihiro Kubozono

Phys. Rev. B **93**, 104508 — Published 8 March 2016

DOI: 10.1103/PhysRevB.93.104508

# Correlation of superconductivity with crystal structure in $(NH_3)_yCs_xFeSe$

**Lu Zheng[1], Xiao Miao[1], Yusuke Sakai[1], Hidenori Goto[1], Eri Uesugi[1], Ritsuko Eguchi[1], Saki Nishiyama[1], Kunihisa Sugimoto[2], Akihiko Fujiwara[3] and Yoshihiro Kubozono[1,4,*]**

[1]Research Laboratory for Surface Science, Okayama University, Okayama 700-8530, Japan

[2]Japan Synchrotron Radiation Research Institute, SPring-8, Hyogo 679-5198, Japan

[3]Department of Nanotechnology for Sustainable Energy, Kwansei Gakuin University, Sanda 669-1337, Japan

[4]Research Centre of New Functional Materials for Energy Production, Storage and Transport, Okayama University, Okayama 700-8530, Japan

*Corresponding author: kubozono@cc.okayama-u.ac.jp

The superconducting transition temperature, $T_c$, of ammoniated metal-doped FeSe, $(NH_3)_yM_xFeSe$ (M: metal atom), has been scaled with the FeSe plane spacing, and it has been suggested that the FeSe plane spacing depends on the location of metal atoms in $(NH_3)_yM_xFeSe$ crystals. Although the crystal structure of $(NH_3)_yLi_xFeSe$ exhibiting a high $T_c$ (~44 K) was determined from neutron diffraction, the structure of $(NH_3)_yM_xFeSe$ exhibiting a low $T_c$ (~ 32 K) has not been determined thus far. Here, we determined the crystal structure of $(NH_3)_yCs_{0.4}FeSe$ ($T_c$ = 33 K) through the Rietveld refinement of the X-ray diffraction (XRD) pattern measured with synchrotron radiation at 30 K. The XRD pattern was analyzed based on two different models, on-center and off-center, under a space group of $I4/mmm$. In the on-center structure, the Cs occupies the 2*a* site and the N of $NH_3$ may occupy either the 4*c* or 2*b* site, or both. In the off-center structure, the Cs may occupy either the 4*c* or 2*b* site, or both, while the N occupies the 2*a* site. Only an on-center structure model in which the Cs occupies the 2*a* and the N of $NH_3$ occupies the 4*c* site provided reasonable results in the Rietveld analysis. Consequently, we concluded that $(NH_3)_yCs_{0.4}FeSe$ can be assigned to the on-center structure, which produces a smaller FeSe plane spacing leading to the lower $T_c$.

## Introduction

The study on metal-doped FeSe is one of the most exciting research subjects, because its superconducting transition temperature ($T_c$) has reached a value greater than 45 K [1-4]. Metal-doped FeSe materials can be synthesized using the high-temperature-annealing method [1,5-8] and liquid-ammonia technique [2-3,9-14], and its $T_c$ can be increased by increasing the FeSe plane spacing [2,4]. On the other hand, it was found that pressure application resulted in a high-$T_c$ phase with the $T_c$ reaching a value greater than 45 K [1,2]. Currently, the highest $T_c$ reported in bulk superconductors of metal-doped FeSe is 49 K at 21 GPa [2]. Even at ambient pressure, the $T_c$ of ammoniated metal-doped FeSe materials has reached 46 K for $(NH_3)_yNa_{0.5}FeSe$ [3]. The insertion of $NH_3$ molecules or ammoniated metal coordinates between the FeSe layers in metal-doped FeSe can increase the FeSe plane spacing to produce a higher $T_c$. From the analogy with the relation between the $T_c$ and interlayer distance in ZrNCl [15] and HfNCl [16], we believe that increasing the lattice constant $c$ (or FeSe plane spacing) increases two-dimensionality (2D) to improve Fermi-surface nesting, which enhances spin fluctuation to reinforce the superconducting pairing interaction [2].

Here, it is important to note that the ionic radius of the metal atom inversely correlates with the $T_c$ [11] because metal atoms such as Rb and Cs with larger ionic radii lead to a smaller FeSe plane spacing and, in turn, lower $T_c$. Our studies on the relationship between $c$ and $T_c$ in $(NH_3)_yM_xFeSe$ clarified that the $T_c$ could be directly scaled with the FeSe plane spacing [2,11]. Therefore, we must investigate the reason why the metal atoms with smaller ionic radius can produce higher FeSe plane spacing. Our previous study on $(NH_3)_yNa_xFeSe$ exhibiting different $T_c$s, 32 and 46 K [3,12,17] suggested that a difference in the location of metal atoms in each phase resulted in a different FeSe plane spacing, leading to a different $T_c$. This was suggested from the analogy of the FeSe plane spacing and $T_c$ of the high-$T_c$ ($T_c$ = 46 K [3,14]) phase in $(NH_3)_yNa_xFeSe$ with those of $(NH_3)_yLi_xFeSe$ ($T_c$ = 44 K [3,10]), while the FeSe plane spacing and $T_c$ of the low-$T_c$ phase ($T_c$ = 32 K [12,17]) with those of $K_xFeSe$ ($T_c$ = 31 K [5]). The Rietveld refinement of the neutron diffraction of $(NH_3)_yLi_xFeSe$ clarified that the Li occupied the 4*c* and 2*b* sites and the N of $NH_3$ occupied the 2*a* site [10]. We call this structure the 'off-center structure' because the Li atom is not located in the 2*a* site (0,0,0). On the other hand, we call the structure of $K_xFeSe$ the 'on-center structure' because the K atom occupies the 2*a* site [5]. We previously reported the crystal structure of $(NH_3)_yCs_xFeSe$ [11] in which the Cs atom occupied the 2*a* site, *i.e.*, the on-center structure, but the $NH_3$ was not included in the analysis. Therefore, a detailed structural analysis for $(NH_3)_yCs_xFeSe$ is indispensable to confirm the scenario in which a metal atom with large ionic radius occupies the 2*a* site.

In this study, we measured the X-ray diffraction (XRD) patterns of $(NH_3)_yCs_{0.4}FeSe$ at different temperatures, and Le Bail fitting was performed to determine the temperature dependence of lattice constants. Furthermore, the Rietveld refinement of the XRD pattern at 30 K was performed using two different models representing the on-center and off-center structures under a space group of $I4/mmm$. Only a Rietveld analysis based on the on-center model provided a reasonable crystal structure, showing that the Cs atom occupied the 2*a* site and the N of $NH_3$ occupied the 4*c* site. The chemical composition was determined to be $(NH_3)_{0.37(4)}Cs_{0.268(4)}FeSe$. In the analysis, a deficiency of Fe was not observed. Furthermore, we investigated the x dependence of $T_c$ in $(NH_3)_yCs_xFeSe$ and discussed the constant $T_c$ value observed from view of the structure.

## Experimental

The β-FeSe sample was prepared using the annealing method described in Ref. 11. The sample of $(NH_3)_yCs_xFeSe$ was synthesized using the liquid-$NH_3$ technique described in Ref. 11 with a nominal x = 0.4. The experimental procedure is the same as that in our previous reports [2,11]. The DC magnetic susceptibilities, *M* / *H*s, of all samples were measured using a SQUID magnetometer (Quantum Design MPMS2); here *M* and *H* refer to the magnetization and applied magnetic field, respectively. The *M* / *H* in this paper corresponds to the mass magnetic susceptibility ($cm^3$ $g^{-1}$ = emu $g^{-1}$). The XRD pattern of the sample was measured with synchrotron radiation (wavelength λ = 0.400176(2) Å) in BL02B2 of SPring-8, Japan. The sample was introduced into a quartz tube and a capillary for *M* / *H* measurement and XRD, respectively, in an Ar-filled glove box ($H_2O$, $O_2$ < 0.1 ppm); the capillary was filled with He gas. Le Bail and Rietveld refinements were performed using the GSAS program.

## Results and Discussion

Figure 1a shows the temperature dependence of magnetic susceptibility (*M* / *H* in $cm^3$ $g^{-1}$) at zero-field cooling (ZFC) and field cooling (FC) for the $(NH_3)_yCs_{0.4}FeSe$ sample. The onset superconducting transition temperature ($T_c^{\mathrm{onset}}$) and $T_c$ were determined to be 35 and 33.5 K, respectively, from the *M* / *H* – *T* plots. As shown in the inset of Figure 1a, the $T_c$ is determined from the cross point of the drop of *M* / *H* and the extrapolation of the normal state. The shielding fraction of the sample was 25% at 10 K. The *M* / *H* – *T* plots suggest the presence of pure β-FeSe which exhibits a $T_c$ as high as 8 K.

Figure 1b shows the XRD patterns measured at different temperatures. These patterns suggest that the crystal structure is the same in the entire temperature range, *i.e.*, no structural phase transition occurs. The Le Bail fitting of the XRD pattern at 30 K is shown in Figure 1c. The Le Bail fitting was achieved assuming the presence of three different crystal phases: $(NH_3)_yCs_xFeSe$, β-FeSe and α-FeSe. The XRD pattern consists of the overlapped peaks from three phases, but some peaks can be assigned to only a single phase among three phases, indicating the presence of three phases. Thus, the XRD pattern could be well analyzed considering the above three phases.

We determined the lattice constants for these crystal phases based on previous reports; the space groups for $(NH_3)_yCs_xFeSe$, β-FeSe and α-FeSe were $I4/\mathrm{mmm}$ (#139) [5,10,11,14], $P4/\mathrm{nmm}$ (#129) [11,18,19] and $P6_3/\mathrm{mmc}$ (#94) [11,20], respectively. The lattice constants, *a* and *c*, were determined to be 3.8082(2) and 16.097(1) Å, respectively, for $(NH_3)_yCs_xFeSe$, and 3.7739(3) and 5.4417(9) Å for β-FeSe, and 3.6166(1) and 5.9233(4) Å for α-FeSe, respectively.

Figure 1d shows the temperature dependence of the *a* and *c* of $(NH_3)_yCs_{0.4}FeSe$. The *a* and *c* at 300 K for $(NH_3)_yCs_{0.4}FeSe$ were determined to be 3.8272(2) and 16.243(1) Å, respectively, which are the same as those, 3.8331(1) and 16.217(1) Å, determined previously by our group [11]. The ratio of lattice constants at 8 K with respect to those at 300 K, *a*(8 K) / *a*(300 K) and *c*(8 K) / *c*(300 K), were 0.994 and 0.989, respectively, suggesting a slightly larger thermal shrinkage along the *c*-direction consisting of van-der Waals interaction between FeSe layers.

Next, we discuss the Rietveld analysis of the XRD pattern of the $(NH_3)_yCs_{0.4}FeSe$ sample at 30 K. The strategy for the Rietveld analysis is schematically shown in Figure 2.

To investigate the validity of the models, the Rietveld analyses were performed using two models (on-center and off-center). In the analysis, the three phases, $(NH_3)_yCs_xFeSe$, β-FeSe and α-FeSe, were included, in the same manner as in the Le Bail fitting (Figure 1c), and the space groups of *I*4/mmm, *P*4/nmm and *P*$6_3$/mmc were adopted for the $(NH_3)_yCs_xFeSe$, β-FeSe and α-FeSe phases, respectively. In all analyses, the structures of β-FeSe and α-FeSe were taken from previous reports [11,18,19,20]. The Fe and Se of $(NH_3)_yCs_xFeSe$ were located at the 4*d* and 4*e* sites, respectively, which are the same as their location in non-ammoniated $K_xFeSe$ [5].

As shown in Figure 2, in the off-center model, the Cs atoms in $(NH_3)_yCs_xFeSe$ are located at the 4*c* (0, 1/2, 0) and 2*b* (0, 0, 1/2) sites, and the N of $NH_3$ was located at the 2*a* site (0, 0, 0); the structure is the same as that of $(NH_3)_yLi_xFeSe$ [10]. The H atom was not included in the analysis throughout this study. The occupancy of Cs and N were refined, while the occupancy of Fe and Se were fixed to 1.0. The Debye-Waller factor $B$ ($B = 8\pi^2U$, $U$: isotropic thermal-displacement of atom) for all atoms (Fe, Se, Cs and N) were refined in the $(NH_3)_yCs_xFeSe$ phase, and $z$ at the 4*e* site (Se) were refined. The refinements of β-FeSe and α-FeSe were performed together with that of $(NH_3)_yCs_xFeSe$. In β-FeSe, the Fe and Se atoms were located at 2*a* (3/4, 1/4, 0) and 2*c* (1/4, 1/4, $z$) sites (choice #2 of *P*4/nmm), respectively, and the $z$ at the 2*c* site and $B$ values at both sites were refined; occupancies at both sites were fixed to 1.0. In α-FeSe, the Fe and Se atoms were located at the 2*a* (0, 0, 0) and 2*c* (1/3, 2/3, 1/4) sites, respectively, and the $B$ values at both sites were refined. The lattice constants of three phases were refined together with background and peak-shape (profile-function) parameters; 'CW profile function 2' of GSAS program was used for the profile function. This function employs a multi-term Simpson's rule integration of the pseudo-Voigt function [21]. The parameters of profile functions are refined independently for each phase.

In the refinement with the off-center model described above, the fractions of $(NH_3)_yCs_xFeSe$, β-FeSe and α-FeSe were evaluated to be 37, 33 and 30%, respectively. The *a* and *c* of $(NH_3)_yCs_xFeSe$ were determined to be 3.8050(3) and 16.066(2) Å, respectively, which are almost the same as those, 3.8082(2) and 16.097(1) Å, evaluated from the Le Bail fitting (Figure 1c). However, the *B* of the Cs at the 4*c* site rapidly increased to 63(12) $Å^2$, while the *B* of the Cs at the 2*b* site had a negative value. Furthermore, the occupancy of N diverged. As a reference, the XRD pattern calculated based on the off-center structure of the $(NH_3)_yCs_xFeSe$ phase and the structures of β-FeSe and α-FeSe is shown in Figure 3a, together with the experimental XRD pattern; the weighted *R* factor (w*R*p) and pattern *R* factor (*R*p) were 11.3 and 7.7%, respectively. From the unreasonable *B* factors and occupancy, we must conclude that this refinement is not successful, showing that the off-center model cannot be applied for the $(NH_3)_yCs_xFeSe$ phase. Logarithmic scale of experimental XRD pattern is shown together with logarithmic-scaled pattern calculated (off-center model) in Figure 3b, to clearly show the entire of XRD pattern.

As shown in Figure 2, we subsequently analyzed the XRD pattern based on the on-center model (space group: *I*4/mmm) for $(NH_3)_yCs_xFeSe$. In the same manner as the analysis based on the off-center model for $(NH_3)_yCs_xFeSe$, β-FeSe and α-FeSe were included in the analysis. The structures of β-FeSe and α-FeSe are the same as those used in the off-center structure analysis. The lattice constants of three phases were refined together with background, and the parameters of profile function were independently refined for each phase; the profile function is the same as that in the off-center model.

In the $(NH_3)_yCs_xFeSe$ phase, the Cs atom was located at the 2*a* (0, 0, 0) site, while the N atom of $NH_3$ was located at the 2*b* (0, 0, 1/2) site. The occupancy of Cs and N were refined, while the occupancy of Fe and Se were fixed to 1.0. The *B* values for all elements and *z* at the 4*e* site were refined in the $(NH_3)_yCs_xFeSe$ phase. The Rietveld refinement showed a negative occupancy and negative *B* for the N atom (2*b* site), indicating that this structure (on-center model) can also be ruled out for the $(NH_3)_yCs_xFeSe$ phase.

Next, in the on-center model, the N atom was moved to the 4*c* (0, 1/2, 0) site from the 2*b* site. The occupancy of Cs and N, *B* values of all elements and *z* of the 4*e* site were refined in this analysis. This analysis successfully provided reasonable values for occupancy, *B* and *z*, as listed in Table 1. The *a* and *c* for $(NH_3)_yCs_xFeSe$ were 3.8075(2) and 16.048(2) Å, respectively, which are the same as those (3.8082(2) and 16.097(1) Å) at 30 K obtained using Le Bail fitting (Figure 1d). The refined structures of β-FeSe and α-FeSe are also reasonable (see Table 1). Consequently, the on-center structure in which the Cs occupies the 2*a* site and the N occupies the 4*c* site was identified for $(NH_3)_yCs_xFeSe$. From the determined occupancies of N and Cs, the chemical stoichiometry was evaluated to be $(NH_3)_{0.37(4)}Cs_{0.268(4)}FeSe$. The x value (0.268(4)) determined from the occupancy of Cs at 2*a* site was consistent with that (x = 0.255(5)) reported previously for the other batch of $(NH_3)_yCs_xFeSe$ (nominal x = 0.4) [11] and was almost consistent with the nominal x value (= 0.4), indicating a reliable occupancy. However, it should be recognized that the occupancy is evaluated under the restriction of *I*4/mmm symmetry.

The fractions of $(NH_3)_yCs_xFeSe$, β-FeSe and α-FeSe was 36, 34 and 32%, respectively. The $wR_p$ and $R_p$ were 10.7 and 7.1%, respectively, indicating a better analysis with on-center model than off-center model. The calculated XRD pattern is shown in Figure 3c, together with the experimental XRD pattern, and logarithmic scale of experimental XRD pattern is shown together with the calculated pattern in Figure 3d, to clearly show the entire of experimental and calculated XRD patterns.

To confirm the on-center structure (Cs: 2*a* site, N: 4*c* site), the N atom was assumed at both the 2*b* and 4*c* sites, and refinement was performed. Consequently, the occupancy for the N at the 2*b* site vanished, and that for the N at the 4*c* site had the same value as that in the analysis based on the on-center model (Cs: 2*a* site, N: 4*c* site) described above. The *B* values of N at the 2*b* and 4*c* sites provided negative and reasonable values, respectively. These results imply that the N does not exist at the 2*b* site; rather, it exists at the 4*c* site. Thus, our analysis of the XRD pattern of the $(NH_3)_yCs_{0.4}FeSe$ sample successfully resulted in the on-center structure (Cs: 2*a* site, N: 4*c* site) for the $(NH_3)_yCs_xFeSe$ phase. The structure suggested for $(NH_3)_yCs_xFeSe$ is shown in Figure 4a. Here we must comment that the fraction of 36% determined from the Rietveld refinement is a little different from the shielding fraction (~25%) from the magnetic susceptibility. Such a deviation is also found in the previous report [11]. One possibility for the lower volume fraction (~25%) determined from magnetic susceptibility is that the presence of non-superconducting / magnetic α-FeSe may suppress the superconducting state. At the present stage, the origin remains to be clarified.

We attempted to determine the occupancy of Fe in the $(NH_3)_yCs_xFeSe$ phase. In the final structure (Table 1 and Figure 4a), only the occupancy and *B* of Fe (4*d* site) were refined to determine the deficiency of Fe, providing the chemical stoichiometry of $(NH_3)_{0.37(4)}Cs_{0.268(4)}Fe_{0.989(4)}Se$. This implies the absence of a deficiency of Fe in $(NH_3)_yCs_xFeSe$, which is reasonable from the low paramagnetic susceptibility observed in the normal state (Figure 1a). Finally, we calculated difference-Fourier-map using the on-center model structure (Cs: 2*a* site, N: 4*c* site), which refers to electron-density-distribution evaluated from the difference between the X-ray diffraction observed and that calculated with on-center model. No electron densities were observed at 2*a* and 4*c* sites, showing clearly that the above on-center model is reasonable. In addition, the electron density was observed at 2*a* site in the difference Fourier map when the N atom was located at 2*a* site (off-center model), indicating the electrons are inefficient, *i.e.*, the element is not N but Cs at 2*a* site. This supports the validity of on-center model.

We tried to determine the anisotropic thermal-displacements, $U_{ij}$'s, for Fe, Se, Cs and N. However, the anisotropic thermal parameters could not be shown, since complete analyses have not been achieved, probably because of an insufficient data quality. Nevertheless, if we shortly comment, the anisotropic parameters, $U_{11}$, $U_{22}$ and $U_{33}$, of N and Cs became negative in the off-center model, while those were positive in on-center model, indicating that the on-center model is suitable.

Furthermore, we evaluated the particle size from *002* reflection, which refer to the particle size along *c* axis. The particle size along *a* axis could not be obtained because all peaks ascribable to *h00* reflection were overlapped from peaks due to other indices. Therefore, we could not compare the particle size between *a* and *c* axes. The particle size (= 27 nm) along *c* axis seems to be a little small, but it is still unclear whether the small particle size originates from two-dimensionality of $(NH_3)_yCs_xFeSe$.

The present structure analysis for $(NH_3)_yCs_xFeSe$ and the previous one for $(NH_3)_yLi_xFeSe$ using neutron diffraction [10] show that the positions of the metal atom and N atom are different between Cs and Li. The *c*, 16.5266(9)Å, of $(ND_{2.8(1)})_{0.5}Li_{0.30(5)}FeSe$ (off-center structure) [10] is larger than that, 16.243(1) Å, of $(NH_3)_{0.37(4)}Cs_{0.268(4)}FeSe$

(on-center structure) determined using Le Bail fitting at 300 K, indicating that the off-center structure leads to an increased FeSe plane spacing, which produces higher $T_c$ because of the increase in the two-dimensionality. Table 2 lists the interatomic distances determined with on-center and off-center models. The interatomic distances can be compared with those in $(NH_3)_yLi_xFeSe$ and $K_xFeSe$ reported previously [5,10]. The interatomic distances determined from off-center model are consistent with those of previous report on $(NH_3)_yLi_xFeSe$ (off-center structure) [5]. On the other hand, the interatomic distances in on-center model could not be compared directly with those of other $(NH_3)_yM_xFeSe$ having on-center structure because of no data, but as seen from Table 2, the Fe - Se and M - Se distances are consistent with those of non-ammoniated $K_xFeSe$ (on-center structure), indicating that the analysis based on the on-center model is reliable.

Here, it is worth noting that the limited x in $(NH_3)_yM_xFeSe$ is 0.5 for the on-center structure since the M occupies 2*a* site, while it increases to 1.5 for the off-center structure since the M can occupy the 2*b* and 4*c* sites. Since the x in $(NH_3)_yCs_xFeSe$ and $(NH_3)_yLi_xFeSe$, as described above, is less than 0.5, they can have both the on-center and off-center structures. Actually, depending on the ionic radius, the structure adopted seems to be different. Our recent study showed that $(NH_3)_yNa_xFeSe$ has two superconducting phases ($T_c$ = 32 K and 46 K [17]) depending on the x value, and the phases have different *c* values (14.145(8) Å for the 32 K phase and 17.565(7) Å for the 46 K phase). A value of x greater than 0.5 produces the high-$T_c$ phase presumably owing to the off-center structure, which is reasonable because a value of x greater than 0.5 is not allowed for the on-center structure. Furthermore, our study showed that $(NH_3)_yLi_xFeSe$ possessed only a single superconducting phase when varying x [17]. Therefore, the x dependence of $T_c$ in

$(NH_3)_yCs_xFeSe$ is of interest because it would directly relate to whether the position of the Cs atom varies with x.

The x dependence of $T_c$ showed that the $T_c$ did not change when varying the nominal x value from 0.0 to 1.3 (Figure 4b) and it was constant at 33 ± 2 K. This indicates that only an on-center structure is adopted in $(NH_3)_yCs_{0.4}FeSe$ and the Cs amount intercalated in the FeSe lattice may be $x \leq 0.5$ despite varying the x value. Only a single phase ($T_c \sim 33$ K) was realized in $(NH_3)_yCs_xFeSe$, which is different from $(NH_3)_yNa_xFeSe$ and $(NH_3)_yLi_xFeSe$, indicating the ionic radius of intercalant is a key for determining the $T_c$, *i.e.*, the larger ionic radius leads to the lower $T_c$.

## Conclusions

The Rietveld refinement of the X-ray diffraction pattern of $(NH_3)_yCs_{0.4}FeSe$ was successfully achieved for the first time, and it revealed an on-center structure in which the Cs and the N of $NH_3$ occupy the 2*a* and 4*c* sites, respectively. This suggests that the low-$T_c$ phase ($T_c \sim 32$ K) found in $(NH_3)_yM_xFeSe$ takes the on-center structure, while the high-$T_c$ phase ($T_c \sim 45$ K) takes the off-center structure, as determined for $(NH_3)_yLi_xFeSe$ [10]. The on-center structure has a smaller FeSe plane spacing than that of off-center structure, and the FeSe plane spacing closely relates to the $T_c$. This study clarified not only the structural difference between the low-$T_c$ and high-$T_c$ phases in $(NH_3)_yM_xFeSe$ but also the effect of the location of the metal and $NH_3$ atoms on the FeSe plane spacing (or $T_c$). As the location of metal atoms with relatively large and small ionic radii (Cs and Li) was determined, the next target for determination must be FeSe materials incorporating a metal atom with intermediate ionic radius such as Na, which produces multiple superconducting phases (high-$T_c$ and low-$T_c$ phases [12,17]). This study constitutes the first step towards clarifying the correlation between the crystal structure and $T_c$ in $(NH_3)_yM_xFeSe$.

## Acknowledgments

This study was partly supported by Grants-in-aid (22244045, 24654105, 26105004) from MEXT, by the LEMSUPER project (JST-EU Superconductor Project) and ACT-C project of the Japan Science and Technology Agency (JST), and by the Program for Promoting the Enhancement of Research Universities. The XRD measurement at SPring-8 was performed under the proposal (2014A1102).

## References

[1] L. L. Sun, X.-J. Chen, J. Guo, P. Gao, Q.-Z. Huang, H. Wang, M. Fang, X. Chen, G. Chen, Q. Wu, C. Zhang, D. Gu, X. Dong, L. Wang, K. Yang, A. Li, X. Dai, H. Mao and Z. Zhao, Nature **483**, 67 (2012).

[2] M. Izumi, L. Zheng, Y. Sakai, H. Goto, M. Sakata, Y. Nakamoto, H. L. Nguyen, T. Kagayama, K. Shimizu, S. Araki, T. C. Kobayashi, T. Kambe, D. Gu, J. Guo, J. Liu, Y. Li, L. Sun, K. Prassides and Y. Kubozono, Sci. Rep. **5**, 9477 (2015).

[3] T. P. Ying, X. L. Chen, G. Wang, S. F. Jin, T. T. Zhou, X. F. Lai, H. Zhang and W. Y. Wang, Sci. Rep. **2**, 426 (2012).

[4] T. Noji, T. Hatakeda, S. Hosono, T. Kawamata, M, Kato and Y. Koike, Physica C **504**, 8 (2014).

[5] J. Guo, S. Jin, G. Wang, S. Wang, K. Zhu, T. Zhou, M. He and X. Chen, Phys. Rev. B **82**, 180520(R) (2010).

[6] A. F. Wang, J. J. Ying, Y. J. Yan, R. H. Liu, X. G. Luo, Z. Y. Li, X. F. Wang, M. Zhang, G. J. Ye, P. Cheng, Z. J. Xiang and X. H. Chen, Phys. Rev. B **83**, 060512(R) (2011).

[7] A. Krzton-Maziopa, Z. Shermadini, E. Pomjakushina, V. Pomjakushin, M. Bendele, A. Amato, R. Khasanov, H. Luetkens and K. Conder, J. Phys.: Condens. Matter **23**, 052203 (2011).

[8] M. Fang, H. Wang, C. Dong, Z. Li, C. Feng, J. Chen and H. Yuan, Europhys. Lett. **94**,

27009 (2011).

[9] T. Ying, X. Chen, G. Wang, S. Jin, X. Lai, T. Zhou, H. Zhang, S. Shen and W. Wang, J. Am. Chem. Soc. **135**, 2951 (2013).

[10] M. Burrard-Lucas, D. G. Free, S. J. Sedlmaier, J. D. Wright, S. J. Cassidy, Y. Hara, A. J. Corkett, T. Lancaster, P. J. Baker, S. J. Blundell and S. J. Clarke, Nature Mater. **12**, 15 (2013).

[11] L. Zheng, M. Izumi, Y. Sakai, R. Eguchi, H. Goto, Y. Takabayashi, T. Kambe, T. Onji, S. Araki, T. C. Kobayashi, J. Kim, A. Fujiwara and Y. Kubozono, Phys. Rev. B **88**, 094521(2013).

[12] Y. Sakai, L. Zheng, M. Izumi, K. Teranishi, R. Eguchi, H. Goto, T. Onji, S. Araki, T. C. Kobayashi and Y. Kubozono, Phys. Rev. B **89**,144509 (2014).

[13] S. J. Sedlmaier, S. J. Cassidy, R. G. Morris, M. Drakopoulos, C. Reinhard, S. J. Moorhouse, D. O'Hare, P. Manuel, D. Khalyavin and S. J. Clarke, J. Am. Chem. Soc. **136**, 630 (2014).

[14] J. G. Guo, H. C. Lei, F. Hayashi and H. Hosono, Nat. Commun. **5**, 4756 (2014).

[15] S. Yamanaka, J. Mater. Chem. **20**, 2922 (2010).

[16] G. Ye, J. Ying, Y. Yan, X. Luo, P. Cheng, Z. Xiang, A. Wang and X. Chen, Phys. Rev. B **86**, 134501 (2012).

[17] L. Zheng, X. Miao, Y. Sakai, M. Izumi, H. Goto, S. Nishiyama, E. Uesugi, Y. Kasahara, Y. Iwasa and Y. Kubozono, Sci. Rep. **5**, 12774 (2015).

[18] F.-C. Hsu, J.-Y. Luo, K.-W. Yeh, T.-K. Chen, T.-W. Huang, P. M. Wu, Y.-C. Lee, Y.-L. Huang, Y.-Y. Chu, D.-C. Yan and M.-K. Wu, Proc. Natl. Acad. Sci. **105**, 14262 (2008).

[19] T. M. McQueen, Q. Huang, V. Ksenofontov, C. Felser, Q. Xu, H. Zandbergen, Y. S. Hor, J. Allred, A. J. Williams, D. Qu, J. Checkelsky, N. P. Ong and R. J. Cava, Phys. Rev. B **79**, 014522 (2009).

[20] T. Hirone and S. Chiba, J. Phys. Soc. Jpn. **11**, 666 (1956).

[21] C. J. Howard, J. Appl. Cryst. 15, 615 (1982).

Table 1. Final crystal structure of $(NH_3)_yCs_{0.4}FeSe$ determined using Rietveld refinement.

1) Phase 1. $(NH_3)_yCs_{0.4}FeSe$

Body-centered tetragonal lattice: *I*4/mmm (No. 139))

Volume fraction: 35.8%

Lattice constants: *a* = 3.8075(2) Å, *c* = 16.048 (2) Å

| | | occupancy | *x* | *y* | *z* | *B* (Å$^2$) |
|---|---|---|---|---|---|---|
| 4*d* | Fe | 1.0 | 0.00000 | 0.50000 | 0.25000 | 0.2(1) |
| 4*e* | Se | 1.0 | 0.00000 | 0.00000 | 0.3436(2) | 0.56(7) |
| 2*a* | Cs | 0.535(7) | 0.00000 | 0.00000 | 0.00000 | 2.1(2) |
| 4*c* | N | 0.37(4) | 0.00000 | 0.50000 | 0.00000 | 12(3) |

2) Phase 2. β-FeSe

Tetragonal lattice: *P*4/nmm (No. 129, choice 2)

Volume fraction: 33.5%

Lattice constant: *a* = 3.7666(8), *c* = 5.458(2) Å

| | | occupancy | *x* | *y* | *z* | *B* (Å$^2$) |
|---|---|---|---|---|---|---|
| 2*a* | Fe | 1.0 | 0.75000 | 0.25000 | 0.00000 | 1.2(3) |
| 2*c* | Se | 1.0 | 0.25000 | 0.25000 | 0.266(1) | 1.4(2) |

3) Phase 3. α-FeSe)

Hexagonal structure: $P6_3$/mmc (No. 194)

Volume fraction: 31.6%

Lattice constant: *a* = 3.6166(3) Å, c= 5.9293(8) Å

| | | occupancy | *x* | *y* | *z* | *B* (Å$^2$) |
|---|---|---|---|---|---|---|
| 2*a* | Fe | 1.0 | 0.00000 | 0.00000 | 0.00000 | 1.5(2) |
| 2*c* | Se | 1.0 | 0.33333 | 0.66667 | 0.25000 | 0.7(1) |

Table 2. Selected interatomic distances and angles in off-center and on-center models for $(NH_3)_yCs_xFeSe$, and those in $(NH_3)_yLi_xFeSe$ (off-center structure) and $K_xFeSe$ (on-center structure). The site where each element occupies is also shown.

| | **off-center model** | **on-center model** | **$(NH_3)_yLi_xFeSe$[a)]** | **$K_xFeSe$[b)]** |
|---|---|---|---|---|
| **Fe - Se (Å)** | 2.4074(2)<br>*4d* - *4e* | 2.4229(1)<br>*4d* - *4e* | 2.408(1)<br>*4d* - *4e* | 2.4406(4)<br>*4d* - *4e* |
| **Se-Fe-Se (°)** | 104.4217(1)<br>*4d* - *4e* - *4d* | 103.5818(1)<br>*4d* - *4e* - *4d* | 104.40(8)<br>*4d* - *4e* - *4d* | 106.600(4)<br>*4d* - *4e* - *4d* |
| **M - N (Å)** | 1.9025(1)<br>*4c* - *2a* | 1.9038(1)<br>*2a* - *4c* | 1.9029(1) *4c* - *2a* | No |
| **M - N (Å)** | 2.6905(1)<br>*2b* - *2a* | No | 2.6912(1)<br>*2b* - *2a* | No |
| **N - Se (Å)** | 3.7010 (3)<br>*2a* – *4e* | 3.1523(3)<br>*2a* – *4e* | 3.7207(1) *2a* – *4e* | No |
| **M - Se (Å)** | 3.1746(3)<br>*4c* - *4e* | 3.6828(2)<br>*2a* - *4e* | 3.1972(1)<br>*4c* - *4e* | 3.4443(4)<br>*2a* - *4e* |
| **M - Se (Å)** | 2.5414(4)<br>*2b* - *4e* | No | 2.5693(1)<br>*2b* - *4e* | No |

a) Taken from ref. 10.

b) Taken from ref. 5.

## Figure caption

Figure 1. (a) *M* / *H* *vs*. *T* plots and (b) temperature-dependent XRD patterns of $(NH_3)_yCs_{0.4}FeSe$. In (b), the peaks due to only a single phase among three phases of $(NH_3)_yCs_{0.4}FeSe$, β-FeSe and α-FeSe are shown by symbols, `+’, ‘#’ and ‘*’, respectively. (c) Le Bail fitting curve (red line) and experimental XRD pattern (x-mark) of $(NH_3)_yCs_{0.4}FeSe$ at 30 K. Ticks indicates the positions of Bragg reflections predicted from the lattice constants suggested for $(NH_3)_yCs_{0.4}FeSe$ (top), β-FeSe (middle) and α-FeSe (bottom). The difference between the Le Bail fitting and experimental XRD is indicated in blue. (d) Lattice constants, *a* and *c*, are plotted as a function of *T*.

Figure 2. Process of Rietveld refinement for the XRD pattern measured at 30 K for $(NH_3)_yCs_{0.4}FeSe$.

Figure 3. Curves (red line) calculated using the Rietveld refinement and the experimental XRD pattern (x-mark) of $(NH_3)_yCs_{0.4}FeSe$ at 30 K. Rietveld refinement was achieved based on (a) the off-center model and (c) the on-center model. Ticks indicates the positions of Bragg reflections predicted from the lattice constants suggested for $(NH_3)_yCs_{0.4}FeSe$ (top), β-FeSe (middle) and α-FeSe (bottom). The difference between the calculated and experimental XRD patterns is indicated in blue. In the inset of (a) and (c), the calculated and experimental XRD pattern (expanded) in high $2\theta$ angle is shown. Logarithmic scale of experimental XRD pattern and logarithmic-scaled pattern calculated using (b) off-center and (d) on-center models.

Figure 4. (a)Schematic crystal structure of $(NH_3)_yCs_{0.4}FeSe$ ultimately determined using the Rietveld refinement. This structure corresponds to the on-center structure. (b) x dependence of $T_c$ in $(NH_3)_yCs_{0.4}FeSe$.

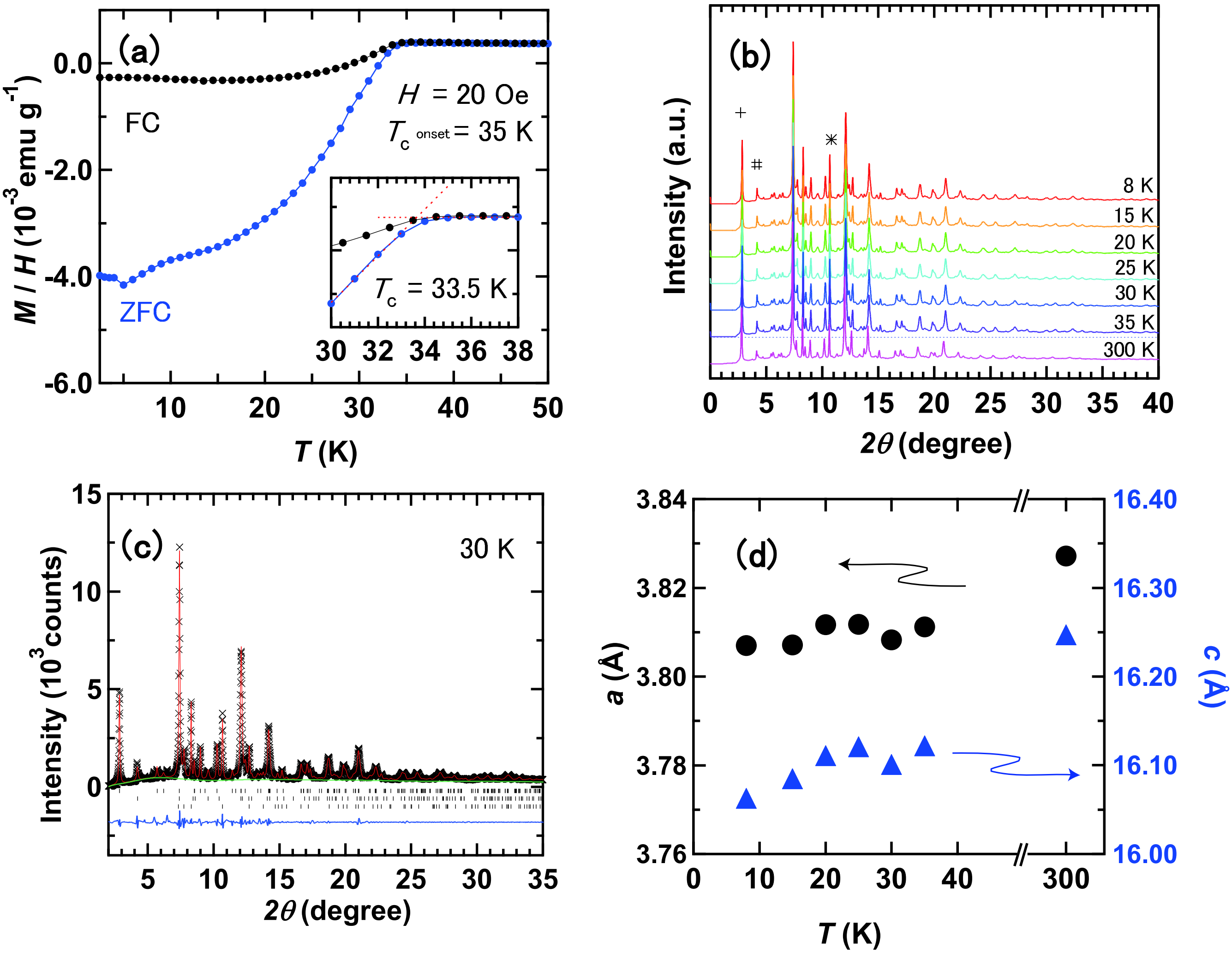

Figure 1 BK12664 11JAN2016

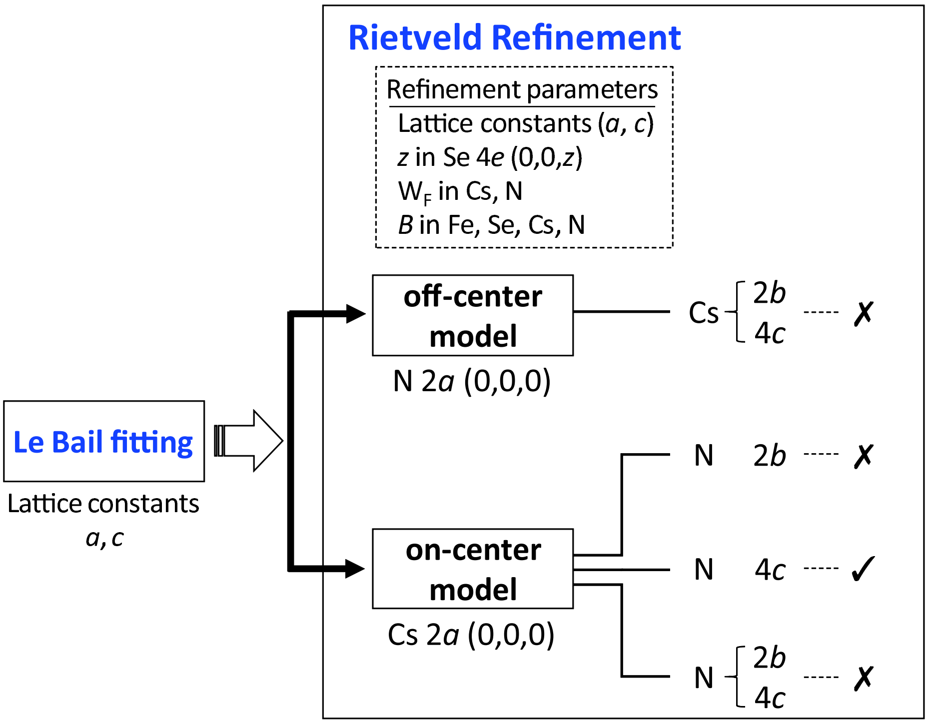

Figure 2 BK12664 11JAN2016

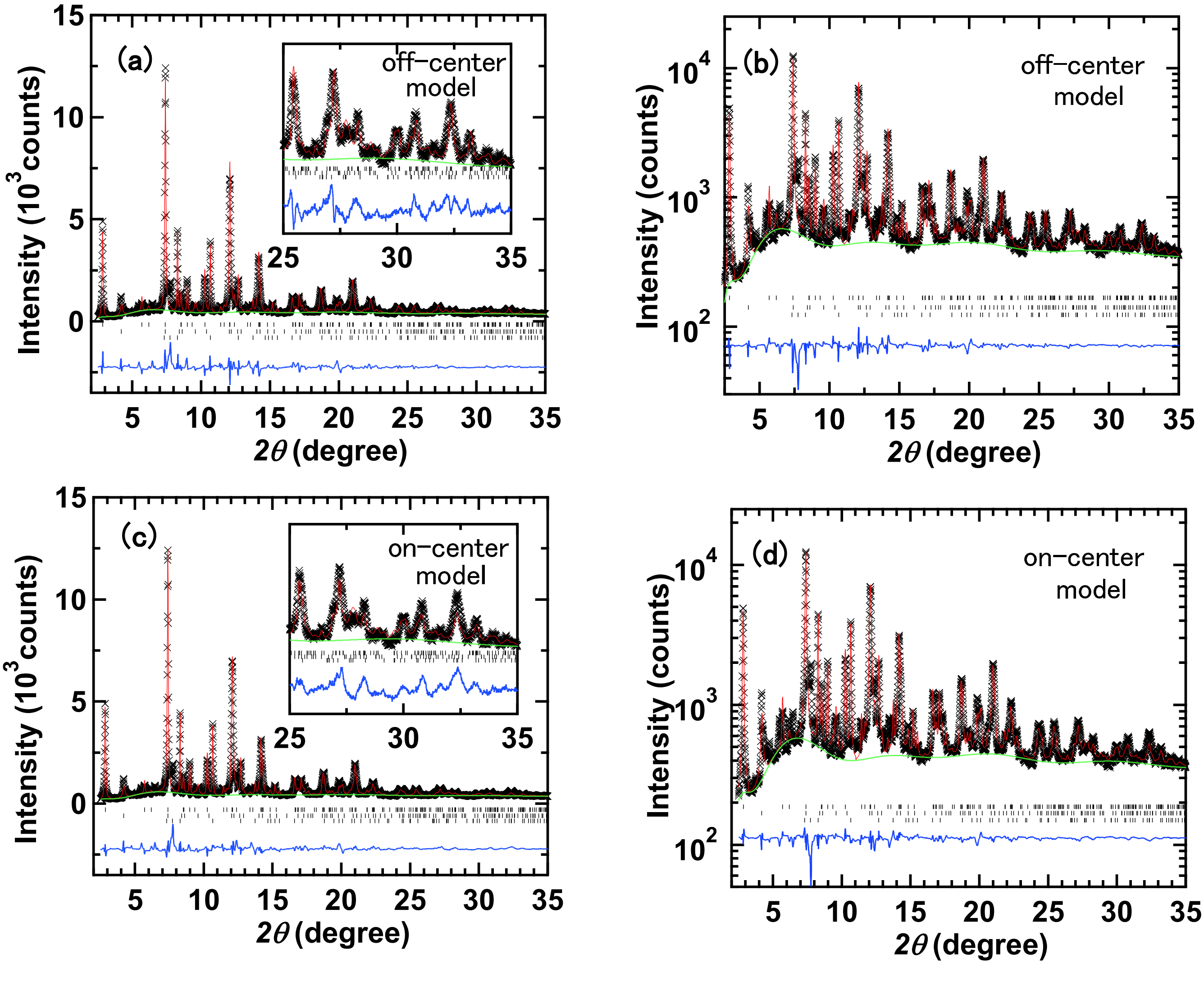

Figure 3    BK12664    11JAN2016

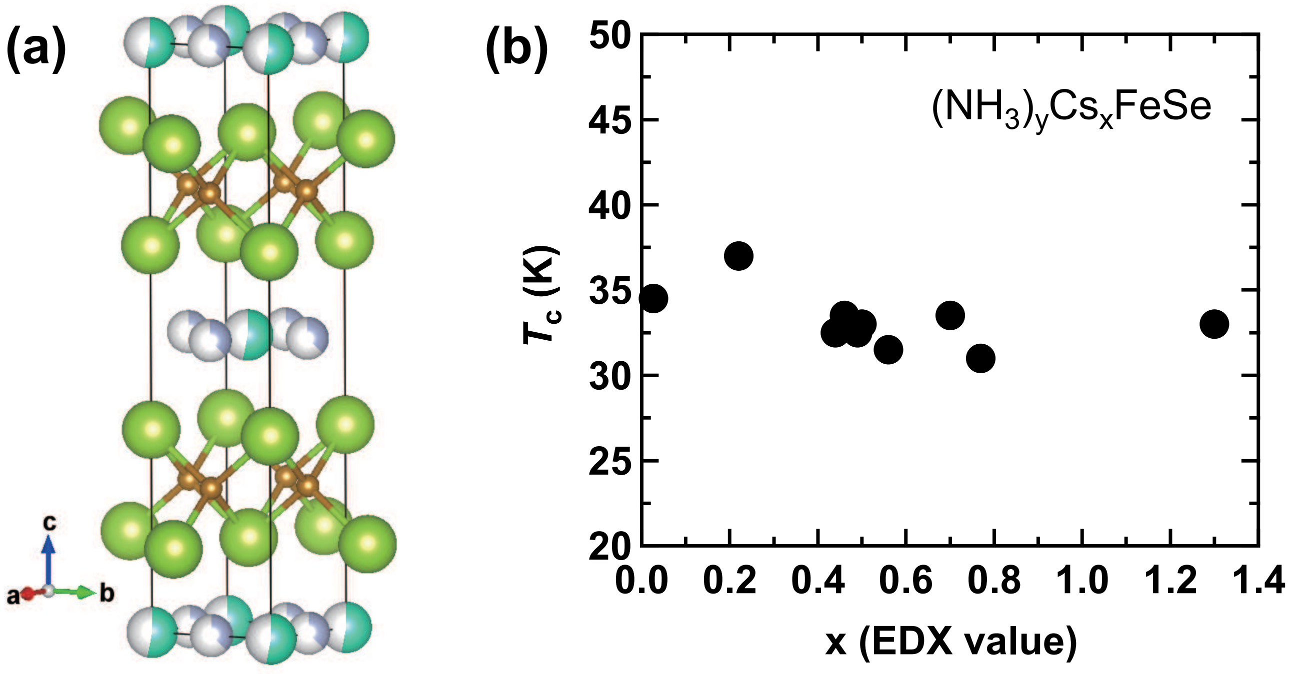

Figure 4 BK12664 11JAN2016